Magnetic Phase Diagram of CuO via High-Resolution Ultrasonic Velocity Measurements

R. Villarreal,[1,*] G. Quirion,[1] M. L. Plumer,[1] M. Poirier,[2] T. Usui,[3] and T. Kimura[3]

[1]*Department of Physics and Physical Oceanography, Memorial University, St. John's, Newfoundland, Canada A1B 3X7*
[2]*Département de Physique, Univesité de Sherbrooke, Sherbrooke, Québec, Canada J1K 2R1*
[3]*Division of Materials Physics, Graduate School of Engineering Science, Osaka University, Toyonaka, Osaka 560-8531, Japan*

(Received 22 May 2012; revised manuscript received 27 July 2012; published 17 October 2012)

High-resolution ultrasonic velocity measurements have been used to determine the temperature—-magnetic-field phase diagram of the monoclinic multiferroic CuO. A new transition at $T_{N3} = 230$ K, corresponding to an intermediate state between the antiferromagnetic noncollinear spiral phase observed below $T_{N2} = 229.3$ K and the paramagnetic phase, is revealed. Anomalies associated with a first order transition to the commensurate collinear phase are also observed at $T_{N1} = 213$ K. For fields with $\mathbf{B} \parallel \mathbf{b}$, a spin-flop transition is detected between 11 T–13 T at lower temperatures. Moreover, our analysis using a Landau-type free energy clearly reveals the necessity for an incommensurate collinear phase between the spiral and the paramagnetic phase. This model is also relevant to the phase diagrams of other monoclinic multiferroic systems.

DOI: 10.1103/PhysRevLett.109.167206 PACS numbers: 75.10.−b, 75.30.Gw, 75.30.Kz, 75.85.+t

Multiferroic phenomena have been a subject of intense interest in recent decades arising from opportunities to explore new fundamental physics as well as possible technological applications [1–3]. Coupling between different ferroic orders has been proven to be driven by different types of mechanisms. In particular, multiferroics with a spiral spin-order-induced ferroelectricity have revealed high spontaneous polarization and strong magnetoelectric coupling [4,5]. Cupric oxide (CuO), the subject of this Letter, was characterized as a magnetoelectric multiferroic four years ago when it was shown that its ferroelectricity is induced by the onset of a spiral antiferromagnetic (AFM) order at an unusually high temperature of 230 K [3]. Thus far, two AFM states have been reported, a low temperature ($T_{N1} \sim 213$ K) AF1 commensurate (CM) collinear state with the magnetic moments along the monoclinic **b** axis and an AF2 incommensurate (ICM) spiral state with half of the magnetic moments in the *ac* plane ($T_{N2} \sim 230$ K) [3,6,7]. However, the authors of the neutron diffraction study [6] questioned the possibility of having a direct condensation from a paramagnetic phase to a spiral magnetic phase in this compound. On the other hand a number of theoretical studies concerning the nature of the magnetic ordering in CuO found this scenario to be possible. Two of these [8,9] are based on Monte Carlo simulations where the direct transition is a consequence of a Dzyaloshinskii-Moriya-type coupling between spin and lattice degrees of freedom [10]. Another analysis of a spin-only Landau-type free energy, expanded to eighth order, gives rise to eleven possible magnetic states [11]. Within a parameter-space phase diagram, a direct transition between the paramagnetic and spiral phases is proposed to explain the observed sequence in CuO. We note that this theory omits any explicit temperature dependence. In contrast, a similar phenomenological model [12] applied to $MnWO_4$ and CuO suggests that there should be an intermediate phase between the spiral and paramagnetic phases.

Encouraged by recent experiments on other multiferroic systems using ultrasonic technique [13], we measured the temperature and field dependence of the velocity of transverse modes in order to determine the magnetic phase diagram of CuO. A new transition is detected at $T_{N3} = 230$ K just above the AF2 spiral phase observed at $T_{N2} = 229.3$ K, while the first order transition is observed at $T_{N1} = 213$ K. Furthermore, dielectric constant measurements confirm that only the spiral phase (between T_{N1} and T_{N2}) supports a spontaneous electric polarization. In addition, we report on a spin-flop transition in the low temperature AF1 collinear phase when $\mathbf{B} \parallel \mathbf{b}$. Thus, based on these findings, a new magnetic-field vs temperature phase diagram is proposed for CuO.

In order to elucidate the possible nature of the AFM states observed in CuO, a nonlocal Landau-type free energy based on a mean-field treatment of a Heisenberg-type Hamiltonian is also developed for CuO and similar monoclinic multiferroics. This approach has been very successful in explaining the magnetic phase diagrams of other multiferroic systems [10,14,15] and includes explicit temperature and magnetic field (B) dependences. In contrast with the conclusions of Refs. [8,9,11], our analysis based on symmetry arguments indicates that there must be a collinear intermediate phase (AF3) between the paramagnetic and spiral AF2 states, as proposed in Ref. [12]. Such a phase has been shown, both theoretically and experimentally, to occur in other geometrically frustrated antiferromagnets [15,16], and recently in multiferroic compounds similar to CuO [17], where symmetry allows for uniaxial anisotropy at second order. Finally, we compare the model predictions with the B-T phase diagram of CuO obtained using ultrasonic velocity data. Similarities with other

multiferroic systems such as $MnWO_4$, $AMSi_2O_6$, $RMnO_3$, RMn_2O_3, and $Ni_3V_2O_8$ are also noted.

For the purpose of this study, a CuO sample was grown using a floating zone technique as described in Ref. [3]. A single crystal was cut with faces perpendicular to the monoclinic axes $\mathbf{a}^*$, $\mathbf{b}^* = \mathbf{b}$, and $\mathbf{c}^*$ ($4 \times 4 \times 3$ mm^3). The sample was then polished to obtain parallel faces. For the velocity measurements, plane acoustic waves were generated using 30 MHz $LiNbO_3$ piezoelectric transducers bonded to opposite faces. Using an ultrasonic interferometer, which measures the phase shift and the amplitude of the first elastic transmitted pulse, high-resolution relative velocity variations ($\Delta V/V \sim 1$ ppm) were achieved. This phase shift corresponds to variations of the elastic constants which reflect changes in the restoring forces between atoms due to magnetoelastic coupling [13,15]. Experimental data presented here were all obtained using the velocity of transverse waves $V_{a^*}[c^*]$ propagating along the $\mathbf{a}^*$ axis and polarized along $\mathbf{c}^*$, with the magnetic field applied along the easy magnetic axis of CuO ($\mathbf{b}$ axis). Simultaneous capacitance measurements were carried out using an AH 2550A Ultra Precision 1 kHz Capacitance Bridge to identify which of these phases are ferroelectric. For that purpose, electrodes were mounted on faces perpendicular to the $\mathbf{b}$ axis in order to determine the dielectric constant ϵ_b.

Figure 1 shows the temperature dependence of the relative sound velocity variations ($\Delta V/V$) for $\mathbf{B} \parallel \mathbf{b}$. At zero field, the anomaly observed at $T_{N1} = 213$ K (see inset of Fig. 1) coincides very well with the onset of a CM collinear antiferromagnetic state. Our high-resolution velocity measurements also reveal *two* anomalies, at $T_{N2} = 229.3$ K and $T_{N3} = 230.0$ K, near the stabilization of a spiral order previously determined by neutron diffraction and susceptibility measurements [3,6], which were thought to occur at a single transition. At higher fields, the amplitude of the steplike variation observed at 229.3 K, as well as the temperature difference between T_{N2} and T_{N3} increases, confirming the existence of a new intermediate magnetic order AF3. This finding is supported by dielectric measurements also shown in Fig. 1. Notice that, as the stability range of the intermediate phase is small ($\Delta T \sim 0.7$ K, which agrees with the prediction of Ref. [12]), velocity and dielectric data have been collected simultaneously to avoid any ambiguity regarding the actual critical temperatures. Thus, as shown in Fig. 1 (for $B = 0$ and 7 T), the anomaly observed on the dielectric constant ϵ_b coincides very well with T_{N2} determined using velocity data, while no variation is noticeable at T_{N3}. These results also indicate that the new phase AF3 is not ferroelectric, while magnetoelectric coupling exists for the AF2 phase.

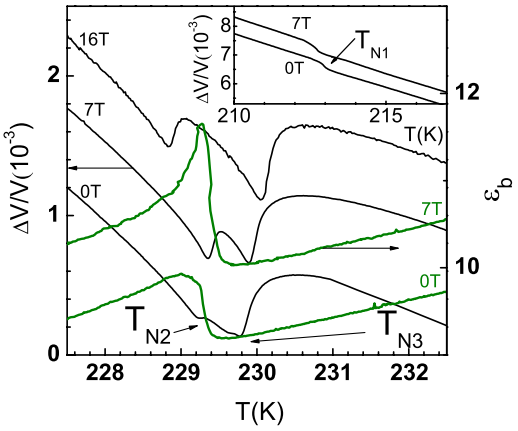

FIG. 1 (color online). Temperature dependence of the dielectric constant ϵ_b (in green, labeled 7 T and 0 T on the right side) and the relative velocity variations of transverse mode $V_{a^*}[c^*]$ measured at different fields with $\mathbf{B} \parallel \mathbf{b}$.

We present in Fig. 2 the magnetic phase diagram of CuO determined up to 16 T for $\mathbf{B} \parallel \mathbf{b}$. The inset of Fig. 2 shows the field dependence of the velocity which displays a minimum around 11 T for $T = 125$ K. As the magnetic moments are known to be parallel to the field in the AF1 CM collinear state [3,6], we attribute this anomaly to a spin-flop transition [18]. In summary, while the critical temperatures T_{N1}, T_{N2}, and T_{N3} are weakly field dependent, the spin-flop critical field B_{SF} increases with temperature. At 10 K, $B_{SF} = 11$ T and increases slowly up to 13.5 T at T_{N1}, in good agreement with magnetic susceptibility measurements performed on powder samples [19].

Since no neutron data exist for the HF1 and AF3 states, we develop a Landau-type model in order to elucidate the nature of these new magnetic orders [15–17]. Only terms invariant with respect to the generators of the space group of the high temperature phase [20] are considered. This approach yields the relevant anisotropic contributions which play a crucial role in the magnetic properties. The integral form of the free energy is expanded in powers of the nonlocal spin density $\mathbf{s}(\mathbf{r})$ defined in terms of a uniform field-induced magnetization $\mathbf{m}$ and a spin polarization vector $\mathbf{S}$ modulated by a single wave vector $\mathbf{Q}$ describing the long-range magnetic order (Eq. (6) of Ref. [15]).

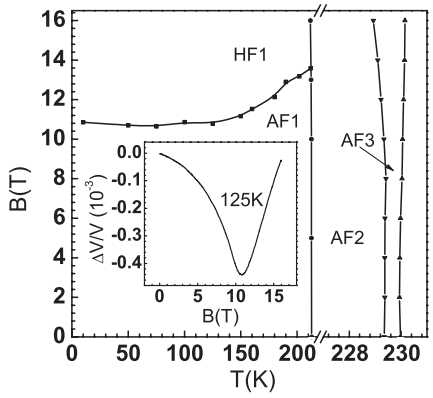

FIG. 2. Magnetic phase diagram of CuO for $\mathbf{B} \parallel \mathbf{b}$. Inset shows the relative velocity variation of $V_{a^*}[c^*]$ as a function of the field for $T = 125$ K.

Within the present model, the value of $\mathbf{Q}$ can be determined directly by considering the isotropic quadratic contribution

$$F_{2I} = \frac{1}{2V^2}\int d\mathbf{r_1} d\mathbf{r_2} A(\mathbf{r_1}-\mathbf{r_2})\mathbf{s}(\mathbf{r_1})\cdot\mathbf{s}(\mathbf{r_2}), \quad (1)$$

which leads to $F_{2I} = \frac{1}{2}\tilde{A}_0 m^2 + A_Q S^2$ where $A_Q = aT + J_Q$, with J_Q being the Fourier transform of the exchange integral $J(\mathbf{R})$. Such a term can be derived from a mean-field treatment of a Heisenberg Hamiltonian [21]. Considering the C-type monoclinic cell with four Cu^{2+} magnetic ions, we obtain

$$\begin{aligned} J(\mathbf{Q}) &= 2[J_1 f_1(\mathbf{Q}) + J_2 f_2(\mathbf{Q}) + J_3 f_3(\mathbf{Q}) + J_4 f_4(\mathbf{Q})] \\ f_1(\mathbf{Q}) &= \cos(\pi q_a - \pi q_c) \\ f_2(\mathbf{Q}) &= \cos(\pi q_a + \pi q_c) \\ f_3(\mathbf{Q}) &= \cos(\pi q_a - \pi q_b) + \cos(\pi q_a + \pi q_b) \\ f_4(\mathbf{Q}) &= \cos(\pi q_b - \pi q_c) + \cos(\pi q_b + \pi q_c), \end{aligned} \quad (2)$$

where J_1 and J_2 represent the nearest-neighbors exchange interactions along the AFM chain (sites 2–3) and between chains (sites 1–4) on the same plane normal to $\mathbf{b}$. The terms J_3 and J_4 represent the exchange interactions along $\mathbf{a}$ (sites 1–2) and $\mathbf{c}$ (sites 1–3) between ions on different planes (see Fig. 3). The value of $\mathbf{Q}$ is then calculated by finding the extrema of J_Q [Eq. (2)] as a function of the exchange interactions. With $J_1 = 1$ and $J_3 = J_4 = 0$ we get the expected CM wave vector $\mathbf{Q}_{\mathrm{CM}} = [\frac{1}{2}\ 0\ -\frac{1}{2}]$ for $J_2 \leq 0$ (ferromagnetic exchange). Moreover, an ICM state with a modulation vector comparable to that of the experimental value $\mathbf{Q}_{\mathrm{ICM}} = [0.5060\ -\ 0.483]$ is stabilized whenever J_3 and/or J_4 are nonzero but small relative to J_1 (for example, $J_2/J_1 = -0.3$, $J_3/J_1 = 0.017$, and $J_4/J_1 = 0$ leading to $J_Q/J_1 = -2.6$). These relative values are in good agreement with estimates from density functional theory [8,22,23] and are consistent with the quasi-1D magnetic character of CuO.

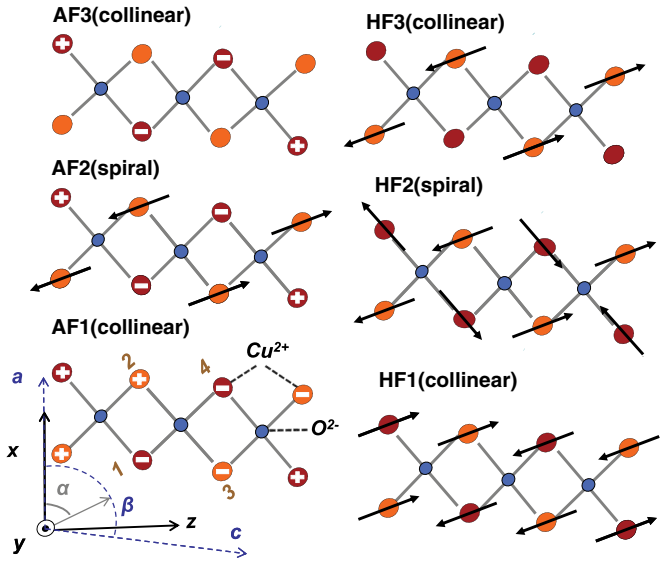

FIG. 3 (color online). Spin configurations in a magnetic cell of 8 ions [red (labeled 1 and 4) and orange (labeled 2 and 3) circles]. Red circles represent magnetic ions at $b = 1/2$. The $+$ ($-$) symbols represent spins in (out) of the page. When no direction is specified (as in AF3 and HF3), spins on these sites are not ordered.

In addition to the usual isotropic second order exchange term, we also consider anisotropic contributions. For monoclinic crystals ($C2/c$), we identified three invariants, written in single-ion form (as they would also appear in a Heisenberg-type Hamiltonian)

$$\begin{aligned} F_{2A} = \frac{1}{2V}\int [&D_y(\mathbf{r})s_y(\mathbf{r})s_y(\mathbf{r}) + D_z(\mathbf{r})s_z(\mathbf{r})s_z(\mathbf{r}) \\ &+ D_{xz}(\mathbf{r})s_x(\mathbf{r})s_z(\mathbf{r})]d\mathbf{r}. \end{aligned} \quad (3)$$

While D_y can be used to set the magnetic easy axis along $\mathbf{b}$, the other terms are necessary in order to define the direction of the moments in the ac plane. Furthermore, to account for noncollinear spin configurations, we parametrize $\mathbf{S} = \mathbf{S_1} + i\mathbf{S_2}$, with

$$\begin{aligned} \mathbf{S_1} &= S\cos\beta[\cos\gamma\hat{\mathbf{y}} + \sin\gamma\hat{\rho}_\mathbf{2}], \\ \mathbf{S_2} &= S\sin\beta[\cos\theta\hat{\rho}_\mathbf{1} + \sin\theta(\cos\gamma\hat{\mathbf{y}} + \sin\gamma\hat{\rho}_\mathbf{2})], \end{aligned} \quad (4)$$

where $\hat{\rho}_\mathbf{1}$ and $\hat{\rho}_\mathbf{2}$ are two orthogonal unit vectors normal to the easy axis, $\hat{\mathbf{y}} \parallel \mathbf{b}$. Thus, the direction of the moments in the ac plane is accounted for by designating the unit vectors $\hat{\rho}_\mathbf{1}$ and $\hat{\rho}_\mathbf{2}$ relative to the lattice vectors, $\hat{\rho}_\mathbf{1} = \cos\alpha\hat{\mathbf{x}} + \sin\alpha\hat{\mathbf{z}}$ and $\hat{\rho}_\mathbf{2} = -\sin\alpha\hat{\mathbf{x}} + \cos\alpha\hat{\mathbf{z}}$. As shown in Fig. 3, the parameter α represents the angle between the ac plane component of $\mathbf{S}$ relative to the monoclinic axis $\mathbf{a} \parallel \hat{\mathbf{x}}$. After integration, all second-order contributions for $\mathbf{m} \parallel \mathbf{H} \parallel \hat{\mathbf{y}}$ reduce to

$$\begin{aligned} F_2^{\mathrm{total}} = &\tfrac{1}{2}\tilde{A}_0 m^2 + A_Q S^2 - \tfrac{1}{2}D_{y0}m^2 - D_{yQ}|S_y|^2 \\ &- D_{zQ}|S_z|^2 + D_{xzQ}S_x S_z - \mathbf{H}\cdot\mathbf{m}. \end{aligned} \quad (5)$$

Adopting the same approach for the fourth-order isotropic term, we obtain

$$\begin{aligned} F_{4I} = &B_1 S^4 + \tfrac{1}{2}B_2|\mathbf{S}\cdot\mathbf{S}|^2 + \tfrac{1}{4}B_3 m^4 + 2B_4|\mathbf{m}\cdot\mathbf{S}|^2 \\ &+ B_5 m^2 S^2 + \tfrac{1}{4}B_U[(\mathbf{S}\cdot\mathbf{S})^2 + \mathrm{c.c.}]\Delta_{4\mathbf{Q},\mathbf{G}}. \end{aligned} \quad (6)$$

Note the umklapp term $\Delta_{4\mathbf{Q},\mathbf{G}}$, which arises directly from the lattice periodicity [10,21]. This term is crucial in order to account for the first order phase transition observed at T_{N1} in CuO where a CM collinear state is stabilized.

The free energy, $F = F_2^{\mathrm{total}} + F_{4I}$, with $A_Q = a(T - T_Q)$ and $\tilde{A}_0 - D_{y0} = a(T - T_0)$, is then numerically minimized. As in Ref. [16], most coefficients are fixed by the analytical solutions associated with phase boundaries of second order transitions. For example, we get $T_Q = 1.18$, $D_{yQ} = 0.02$, $B_1 = 0.103$, and $B_2 = 0.011$, using reasonable values for the critical temperatures at zero

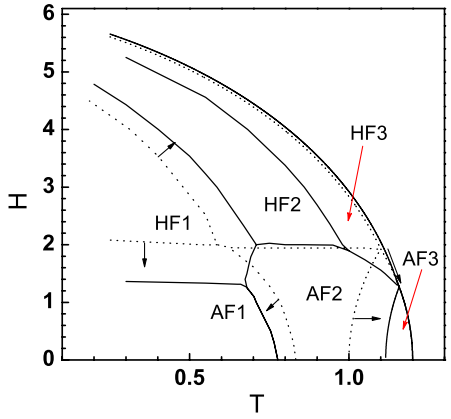

FIG. 4 (color online). Magnetic field—temperature phase diagram of CuO for $\mathbf{H} \parallel \mathbf{b}$ derived from the Landau free energy. Dotted lines represent a prediction with only one anisotropic term included, D_{yQ}. The solid line is for the case where all anisotropic terms are considered.

field ($T_{N3} = 1.2$ and $T_{N2} = 1.12$). We also set $D_{zQ} = 0.01$ as we must have $D_{zQ} < D_{yQ}$, while the direction of the spins in the ac plane ($\alpha_{\text{exp}} \sim 70°$) [1] determines the ratio $D_{xzQ}/D_{zQ} = -0.42$. The last coefficients are solved with the temperature of the multicritical point (where T_{N2} and T_{N3} boundaries meet) and the maximum field at $T = 0$ K. From this exercise, we find $B_3 = 0.063$ and $B_4 = 0.013$, while $B_5 = 0.1$ was adjusted arbitrarily. Finally, $B_U = 0.035$ is used to obtain $T_{N1} = 0.77$.

Figure 4 shows the magnetic phase diagram resulting from minimization of the free energy. For comparison, we also present results obtained without the anisotropic terms D_{zQ} and D_{xzQ} (dotted lines). Depending on the scenario considered, we find 5 or 6 magnetic phases illustrated in Fig. 3 and described by the order parameters listed in Table I. At zero field, both models (with and without D_z and D_{xz}) predict the same phase sequence, consistent with our experimental observations shown in Fig. 2. At low temperatures, a collinear phase AF1 with the moments along $\mathbf{b}$ is predicted (see Fig. 3) while the AF2 phase corresponds to a spiral configuration in agreement with neutron scattering data [6]. According to our numerical calculations, the new intermediate phase AF3 is associated with a collinear phase where only half of the moments order with $\mathbf{S} \parallel \mathbf{b}$. As the field is applied, two spin-flop transitions (AF1 → HF1 and AF2 → HF2) are found.

TABLE I. Order parameters.

State	β	θ	γ	α
AF1	$\pi/4$	$\pi/2$	0	...
AF2	β	0	0	70°
AF3	...	...	0	...
HF1	$\pi/4$	$\pi/2$	$\pi/2$	160°
HF2	β	0	$\pi/2$	70°
HF3	$\pi/2$	0	...	70°

The comparison of both phase diagrams indicates that the role of the anisotropic terms D_{zQ} and D_{xzQ} is to reduce the critical field of the AF1 → HF1 transition, decrease the stability range of the intermediate phase AF3, and lead to a new magnetic order HF3 in which half the moments align into the ac plane. These results could account for the fact that no spin-flop phase transition has been observed experimentally up to 16 T for the spiral phase AF2.

Our principal conclusions are that a new collinear phase (AF3) has been detected by high-resolution ultrasonic velocity measurements which occurs between the paramagnetic and the previously identified spiral phase in agreement with a recent prediction [12]. The magnetic-field vs temperature phase diagram for $\mathbf{B} \parallel \mathbf{b}$ has also been determined, revealing the existence of a new spin-flop phase (HF1). Complementary dielectric measurements confirm that magnetoelectric effects only exist in the non-collinear phase. Verification that the new AF3 phase must exist is achieved by a Landau-type model based on a Heisenberg-type Hamiltonian and symmetry arguments. In contrast with the previous MC simulations of Refs. [8,9], which omit anisotropic contributions, we find that spin-lattice coupling is not required to account for the observed magnetic ordering.

Our findings imply that the multiferroic mechanism in CuO is similar to a traditional cycloidal spin-driven type, such as in $MnWO_4$ [12]. The three zero-field magnetically ordered states are stabilized by spin-only contributions which include frustrated exchange interactions [24], spin-orbit induced anisotropy, and an umklapp-type mechanism giving rise to the lower temperature CM phase. This is observed in a number of multiferroic compounds, such as $RMnO_3$ and RMn_2O_5 [25–27], and the kagome compound $Ni_3V_2O_8$ [28]. Our model accounts for the experimental phase diagram of CuO determined in this work and is potentially useful for the description of other monoclinic multiferroic systems, in particular $MnWO_4$ [29] and $AMSi_2O_6$ [30]. Let us point out that, according to the Dzyaloshinskii-Moriya interaction, the field-induced spiral phase (HF2) could also be magnetoelectric. However, in this case the electric polarization would be in the ac plane, leading to a reduction in the crystal symmetry.

This work was supported by the Natural Science and Engineering Research Council of Canada (NSERC).

*Present address: Department of Condensed Matter Physics, NCCR Materials with Novel Electronic Properties, University of Geneva, 24 Quai Ernest Ansermet, CH-1211 Geneva 4, Switzerland.
renan.villarreal@unige.ch

[1] M. Ain, A. Menelle, B. M. Wanklyn, and E. F. Bertaut, J. Phys. Condens. Matter **4**, 5327 (1992).
[2] M. Fiebig, J. Phys. D **38**, R123 (2005).

[3] T. Kimura, Y. Sekio, H. Nakamura, T. Siegrist, and A. P. Ramirez, Nature Mater. **7**, 291 (2008).
[4] T. Kimura, T. Goto, H. Shintani, K. Ishizaka, T. Arima, and Y. Tokura, Nature (London) **426**, 55 (2003).
[5] K. Wang, J.-M. Liu, and Z. Ren, Adv. Phys. **58**, 321 (2009).
[6] J. B. Forsyth, P. J. Brown, and B. M. Wanklyn, J. Phys. C **21**, 2917 (1988).
[7] P. Babkevich, A. Poole, R. D. Johnson, B. Roessli, D. Prabhakaran, and A. T. Boothroyd, Phys. Rev. B **85**, 134428 (2012).
[8] G. Giovannetti, S. Kumar, A. Stroppa, J. van den Brink, S. Picozzi, and J. Lorenzana, Phys. Rev. Lett. **106**, 026401 (2011).
[9] G. Jin, K. Cao, G.-C. Guo, and L. He, Phys. Rev. Lett. **108**, 187205 (2012).
[10] M. L. Plumer, Phys. Rev. B **78**, 094402 (2008).
[11] P. Tolédano, N. Leo, D. D. Khalyavin, L. C. Chapon, T. Hoffmann, D. Meier, and M. Fiebig, Phys. Rev. Lett. **106**, 257601 (2011).
[12] V. P. Sakhnenko and N. V. Ter-Oganessian, Crystallogr. Rep. (Transl. Kristallografiya) **57**, 112 (2012).
[13] G. Quirion, M. L. Plumer, O. A. Petrenko, G. Balakrishnan, and C. Proust, Phys. Rev. B **80**, 064420 (2009).
[14] S. G. Condran and M. L. Plumer, J. Phys. Condens. Matter **22**, 162201 (2010).
[15] G. Quirion, X. Han, and M. L. Plumer, Phys. Rev. B **84**, 014408 (2011).
[16] M. L. Plumer, K. Hood, and A. Caillé, Phys. Rev. Lett. **60**, 45 (1988).
[17] S. Matityahu, A. Aharony, and O. Entin-Wohlman, Phys. Rev. B **85**, 174408 (2012).
[18] G. Quirion, X. Han, M. L. Plumer, and M. Poirier, Phys. Rev. Lett. **97**, 077202 (2006).
[19] O. Kondo, M. Ono, E. Sugiura, K. Sugiyama, and M. Date, J. Phys. Soc. Jpn. **57**, 3293 (1988).
[20] J. Tolédano and P. Tolédano, *The Landau Theory of Phase Transitions: Application to Structural, Incommensurate, Magnetic, and Liquid Crystal Systems*, World Scientific Lecture Notes in Physics (World Scientific, Singapore, 1987), ISBN 9789971500252.
[21] M. L. Plumer, Phys. Rev. B **44**, 12376 (1991).
[22] X. Rocquefelte, M.-H. Whangbo, A. Villesuzanne, S. Jobic, F. Tran, K. Schwarz, and P. Blaha, J. Phys. Condens. Matter **22**, 045502 (2010).
[23] A.-M. Pradipto, R. Maurice, N. Guihéry, C. de Graaf, and R. Broer, Phys. Rev. B **85**, 014409 (2012).
[24] P. Tolédano, B. Mettout, W. Schranz, and G. Krexner, J. Phys. Condens. Matter **22**, 065901 (2010).
[25] D. O'Flynn, C. V. Tomy, M. R. Lees, A. Daoud-Aladine, and G. Balakrishnan, Phys. Rev. B **83**, 174426 (2011).
[26] T. Kimura, G. Lawes, T. Goto, Y. Tokura, and A. P. Ramirez, Phys. Rev. B **71**, 224425 (2005).
[27] Y. Noda, H. Kimura, M. Fukunaga, S. Kobayashi, I. Kagomiya, and K. Kohn, J. Phys. Condens. Matter **20**, 434206 (2008).
[28] G. Lawes *et al.*, Phys. Rev. Lett. **95**, 087205 (2005).
[29] V. Felea, P. Lemmens, S. Yasin, S. Zherlitsyn, K. Y. Choi, C. T. Lin, and C. Payen, J. Phys. Condens. Matter **23**, 216001 (2011).
[30] S. Jodlauk, P. Becker, J. A. Mydosh, D. I. Khomskii, T. Lorenz, S. V. Streltsov, D. C. Hezel, and L. Bohatý, J. Phys. Condens. Matter **19**, 432201 (2007).